Journal of Applied Polymer Science

Preparation of poly(propylene carbonate)/nano calcium carbonate composites and their supercritical carbon dioxide foaming behavior

Peng Yu,[1,2] Hao-Yang Mi,[1] An Huang,[1] Xian Liu,[1] Bin-Yi Chen,[1] Shui-Dong Zhang,[2] Xiang-Fang Peng[1]

[1]National Engineer Research Center of Novel Equipment for Polymer Processing, South China University of Technology, Guangzhou 510640, People's Republic of China

[2]Key Laboratory of Polymer Processing Engineering (Ministry of Education), South China University of Technology, Guangzhou 510640, People's Republic of China

Correspondence to: X. F. Peng (E-mail: pmxfpeng@scut.edu.cn) and S. D. Zhang (E-mail: starch@scut.edu.cn)

ABSTRACT: Biodegradable polymer foams are attracting extensive attention in both academic and industrial fields. In this study, an emerging biodegradable polymer, poly(propylene carbonate) (PPC), was compounded with nano calcium carbonate (nano-$CaCO_3$) and foamed via supercritical carbon dioxide for the first time. Four concentrations of nano-$CaCO_3$, 1, 3, 5, and 10 wt %, were used and the thermal properties of PPC/nano-$CaCO_3$ composites were investigated. The glass-transition temperature and thermal decomposition temperature of the PPC/nano-$CaCO_3$ composites increased with the addition of nano-$CaCO_3$. The morphologies of the PPC/nano-$CaCO_3$ composites and the rheological results showed that homogeneous dispersions of nano-$CaCO_3$ and percolated nano-$CaCO_3$ networks were achieved at a nano-$CaCO_3$ content of 3 wt %. Therefore, the finest cell diameter (3.13 μm) and highest cell density (6.02×10^9 cells/cm^3) were obtained at the same nano-$CaCO_3$ content. The cell structure dependences of PPC and PPC with a nano-$CaCO_3$ content of 3 wt % (PPC-3) foams on the foaming pressure and temperature were investigated as well. The results suggested that the cell structure of PPC-3 was more stable at different foaming conditions due to the networks of nano-$CaCO_3$. Moreover, the change in pressure was more influential on the cell structure than the temperature. © 2015 Wiley Periodicals, Inc. J. Appl. Polym. Sci. **2015**, *132*, 42248.

KEYWORDS: biodegradable; composites; foams; morphology; rheology

Received 25 November 2014; accepted 20 March 2015

DOI: 10.1002/app.42248

INTRODUCTION

Polymer foams have been extensively used in many fields because of their advantages of light weight, buoyancy, cushioning performance, thermal and acoustic insulation, impact damping, and cost reduction. In particular, biodegradable polymer foams, such as poly(lactic acid) foams, poly(propylene carbonate) (PPC) foams, and poly(ε-caprolactone) foams, have attracted great attention from both industrial and academic areas. The reasons are increasing concerns over the environmental influence and sustainability of petroleum-based polymer materials.[1–7] Among these biodegradable polymers, PPC, which can be synthesized from propylene oxide and carbon dioxide (CO_2), is attracting more and more attention because of concerns about reducing greenhouse gas pollution. The ester bonds in the PPC macromolecular backbone chains supply the high molecular chain flexibility and good melt flow characteristics. However, the poor thermal stability and mechanical properties of PPC have limited its applications.[8]

Recently, great efforts have been devoted to improving the deficient thermal and mechanical properties of PPC.[9,10] PPC reinforced by fillers such as graphene oxide,[11,12] montmorillonite,[13,14] lignocelluloses fiber,[15] glass fiber,[16] calcium carbonate ($CaCO_3$)[17] have been studied and reported. Among these fillers, nano calcium carbonate (nano-$CaCO_3$) has gained much attention because of its high specific surface area and low cost.[18,19] Furthermore, nano-$CaCO_3$ can also increase the melt viscosity of the matrix and act as a bubble nucleating agent, which is conducive to foaming. Therefore, polymer foams filled with $CaCO_3$ have been extensively studied.[20–22] Meng *et al.*[23] prepared PPC/$CaCO_3$ foams with azodicarbonamide as the blowing agent. The addition of $CaCO_3$ to PPC can result in a well-developed and uniform cellular foam structure with a small cell diameter and high cell density. However, azodicarbonamide is a low-molecular-weight organic chemical compound with which it is typically hard to achieve a homogeneous dispersion within the polymer matrix, and the residual of azodicarbonamide has been a problem that is hard to overcome. Supercritical fluid

foaming technology as an environmentally friendly foaming process has received great emphasis recently. In particular, supercritical carbon dioxide (sc-CO_2) has emerged as an important supercritical fluid because of its many desirable attributes, including its nontoxicity, nonflammability, chemical inertia, and moderate critical point (31.1°C and 7.38 MPa). It has been reported that the pore structure of foam can be easily controlled by optimization of the processing parameters, including the saturation pressure (P_s), saturation temperature (T_s), and saturation time.[24–26]

On the basis of the aforementioned advantages of PPC, nano-$CaCO_3$, and sc-CO_2 foaming, in this study, PPC/nano-$CaCO_3$ composites were prepared at various nano-$CaCO_3$ contents and foamed with sc-CO_2 as a physical blowing agent. The dispersability of nano-$CaCO_3$ within the PPC matrix and the effects of nano-$CaCO_3$ on the thermal and rheological properties of the composites were investigated. Furthermore, the composites were foamed, and the effects of the nano-$CaCO_3$ loading level, P_s, and foaming temperature on the cell diameter and cell density were studied.

EXPERIMENTAL

Materials

PPC was purchased from Tai Zhou Bang Feng Plastic Co., Ltd., with a number-average molecular weight of 90,000 and a density of 1.25 g/cm^3. Neat nano-$CaCO_3$ and nano-$CaCO_3$ coated with stearic acid were supplied by Ja Wei Chemical Industrial Co., Ltd.; the average size of neat nano-$CaCO_3$ was 80 nm, and its density was about 2.5 g/cm^3 according to the technical data sheet. The particle size of the stearic acid modified nano-$CaCO_3$ (CCR) was measured by scanning electron microscopy (SEM) in this study. Commercial-purity-grade CO_2 (purity = 99%, Air Liquide) was used as a physical blowing agent.

Nanocomposite Preparation

A corotating triple-screw extruder (IEGTC-25/40, Guangzhou POTOP Co., Ltd., China) equipped with a volumetric feeder and a strand pelletizer was used to compound PPC with nano-$CaCO_3$ particles modified by stearic acid. Only modified nano-$CaCO_3$ particles were used in this study because it has been reported extensively that stearic acid modification could improve the compatibility between the polymer matrix and nanoparticles.[27,28] The extruder had a screw diameter of 25 mm and a length-to-diameter ratio of 40. The temperature profile in the extruder was set at 150°C in the feeding zone, sequentially at 160–160–165–165–165–165–160–155°C in the metering zone, and 150°C at the die. The feeding rate and triple screw rotation speed were set at 9 and 50 rpm, respectively. Before compounding, PPC and nano-$CaCO_3$ were dried at 50 and 100°C in a vacuum oven for 24 h to remove moisture, respectively. Determined amounts of PPC and nano-$CaCO_3$ were manually mixed by tumbling in a plastic ziplock bag and subsequently fed into the extruder. The strands were cooled in a water bath and subsequently granulated by a pelletizer. A series of nanocomposites with nano-$CaCO_3$ contents of 1, 3, 5, and 10 wt % were obtained, and these were labeled PPC-1, PPC-3, PPC-5, and PPC-10, respectively. For comparison, neat PPC was subjected to the same extrusion process to ensure the same thermal history as the PPC/nano-$CaCO_3$ composites. The composites prepared were melt-pressed into sheets of 200 × 80 × 1 mm^3 at 160°C by a press vulcanizing machine (QLB-25D/Q, Wuxi No. 1 Rubber & Plastic Machinery Factory, China) and then cut into small specimens with dimensions of 30 × 10 × 1 mm^3 for the foaming process.

Preparation of Polymeric Foams

The neat PPC and PPC/nano-$CaCO_3$ composites were placed in a high-pressure vessel and heated to T_s (40 or 50°C) for 5 min. Then, the vessel was flushed with low-pressure CO_2 for 3 min via a syringe pump (ISCO-260D); this was followed by the compression of CO_2 to a desired P_s (10 or 20 MPa). The system was kept at equilibrium at T_s and P_s for a desired saturation time (2 h) to ensure CO_2 adsorption equilibrium. Then, the vessel was depressurized to atmospheric pressure quickly for 0.5 s to trigger cell nucleation and cell growth. The vessel was then cooled to ambient temperature rapidly by the circulation of water to maintain the foamed structure.

Characterization

Fourier transform infrared (FTIR) spectroscopy analysis was performed on neat nano-$CaCO_3$ and stearic acid coated nano-$CaCO_3$ particles with a Thermo Nicolet Nexus 670 spectrometer. The particles were pressed with KBr powder into thin films for the test. The FTIR spectra were recorded from 400 to 4000 cm^{-1} with a resolution of 2 cm^{-1} and with 32 scans in transmission mode. One sample of each group was tested for FTIR spectroscopy.

Differential scanning calorimetry (DSC) was conducted on the neat PPC and PPC/nano-$CaCO_3$ composites to investigate their thermal properties with a Netzsch DSC 204 F1 (Germany). Weighted samples were sealed in aluminum pans and heated to 65°C at a rate of 10°C/min under a nitrogen atmosphere. Three samples of each composite group were tested, and the reported results are the average values.

The thermal stability of the PPC and PPC/nano-$CaCO_3$ composites was tested via thermogravimetric analysis (TGA; TG209 F3, Netzsch, Germany). The samples were heated from 30 to 600°C at a heating rate of 10°C/min under a nitrogen atmosphere. Three samples of each composite group were tested, and the reported results are the average values.

The dynamic rheological properties of the neat PPC and PPC/nano-$CaCO_3$ composites were measured with a modular compact rheometer (MCR 302, Anton Paar, Austria) with parallel-plate geometry and 25-mm diameter plates. The tests were performed in an oscillatory mode at 150°C to conduct dynamic frequency sweeps. The complex viscosity (η^*), storage modulus (G'), and loss modulus (G'') as a function of the angular frequency (ω), which ranged from 0.01 to 100 rad/s, were measured. A fixed strain of 1% was used to ensure that the measurements were carried out within the linear viscoelastic range of the samples investigated.

SEM (Nano 430, FEI) was used to observe the dispersion of the nano-$CaCO_3$ in the PPC matrix and the cell morphologies of the foamed samples. The foamed samples were freeze-fractured in liquid nitrogen and gold-sputtered. Both the cell diameter

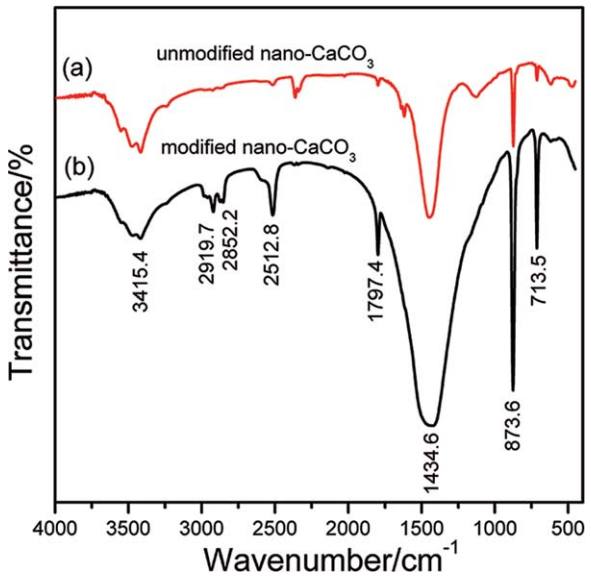

Figure 1. FTIR spectra of the (a) unmodified nano-$CaCO_3$ and (b) CCR. [Color figure can be viewed in the online issue, which is available at wileyonlinelibrary.com.]

and density were determined from the SEM micrographs with Image Pro Plus software. The statistical results of each sample were measured from 3 to 5 differences in the SEM micrographs. The cell density (N_0; cells/cm^3), the number of cells per cubic centimeter of foamed polymer, was determined from eq. (1):[22]

$$N_0 = \frac{6\left[1-\left(\rho_f/\rho_P\right)\right]}{\pi D^3}\times 10^{12} \quad (1)$$

where D is the average cell diameter (μm) and ρ_p (g/cm^3) and ρ_f (g/cm^3) are the mass densities of the sample before and after foaming, respectively, which were measured by the water displacement method in accordance with ASTM D 792.

RESULTS AND DISCUSSION

Nano-$CaCO_3$ Particle Characterization

Steric acid modified nano-$CaCO_3$ particles were used in this study because it has been reported extensively that the modification of nano-$CaCO_3$ particles could improve the filler dispersion within the polymer matrix and significantly enhance the compatibility of nano-$CaCO_3$ with the polymer matrix.[19] FTIR spectroscopy was used in this study to inspect the pristine nano-$CaCO_3$ and steric acid modified nano-$CaCO_3$; the test results are shown in Figure 1. Three strong peaks at 1434, 873, and 713 cm^{-1} corresponded to the asymmetric stretching, out-of-plane bending, and in-plane bending vibrations of CO_3^{2-}, respectively. The 3415-cm^{-1} band was characteristic of the stretching vibrations of O—H, probably because of the influence of water. Two new bands at 2919 and 2852 cm^{-1} appeared in the spectrum of the modified nano-$CaCO_3$; these corresponded to the —CH_2— stretching vibrations of stearic acid. The band at 1797 cm^{-1} was ascribed to the stretching vibrations of C═O from the RCOO group;[29] this illustrated that stearic acid was coated on the nano-$CaCO_3$ particles.

Figure 2 shows the morphology of the nano-$CaCO_3$ particles after modification. We observed that the nano-$CaCO_3$ still presented as individual particles after modification. The measured average particle size results indicate that the nano-$CaCO_3$ size increased slightly after modification from 80 to 83.7 nm, and the distribution of the particle size obeyed Gaussian distribution. Therefore, the steric acid modification procedure altered the surface properties of the nano-$CaCO_3$ particles without obvious changes in the particle size and morphology.

Dispersion of Nano-$CaCO_3$ in the PPC Matrix

The morphology and dispersion of nano-$CaCO_3$ particles in the polymer matrix were the key factors influencing the physical properties and foaming behaviors of the polymer matrix.[22] Figure 3 shows the SEM images of the PPC/nano-$CaCO_3$ composites with various nano-$CaCO_3$ contents. As shown in Figure 3, the nano-$CaCO_3$ particulates distributed in the PPC matrix were seen as dark holes and bright irregularly particles. Most of the nano-$CaCO_3$ particles were scattered on the nanometer scale, and some nano-$CaCO_3$ particles were aggregated and dispersed evenly in the matrix for the PPC-1 and PPC-3 samples. However, some large aggregations were observed in the PPC-5 and PPC-10 samples, as indicated in Figure 3(c,d) by the cycles

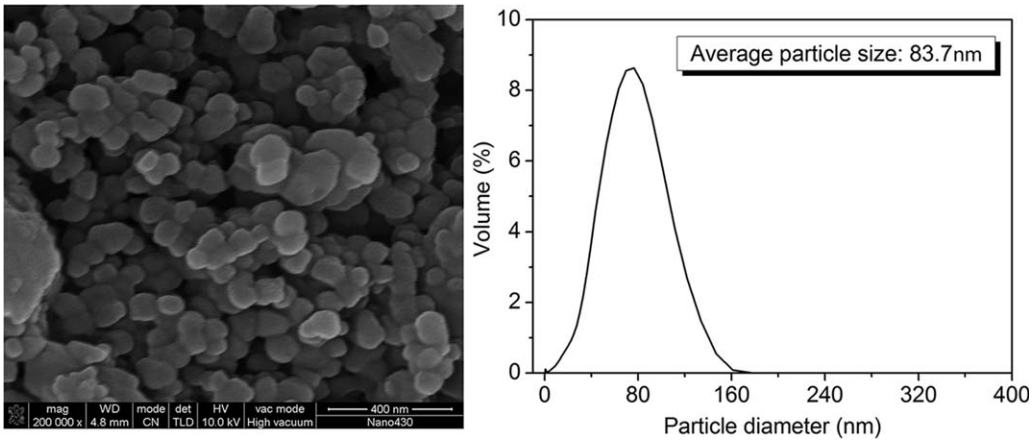

Figure 2. SEM image of the CCR and particle size distribution curve.

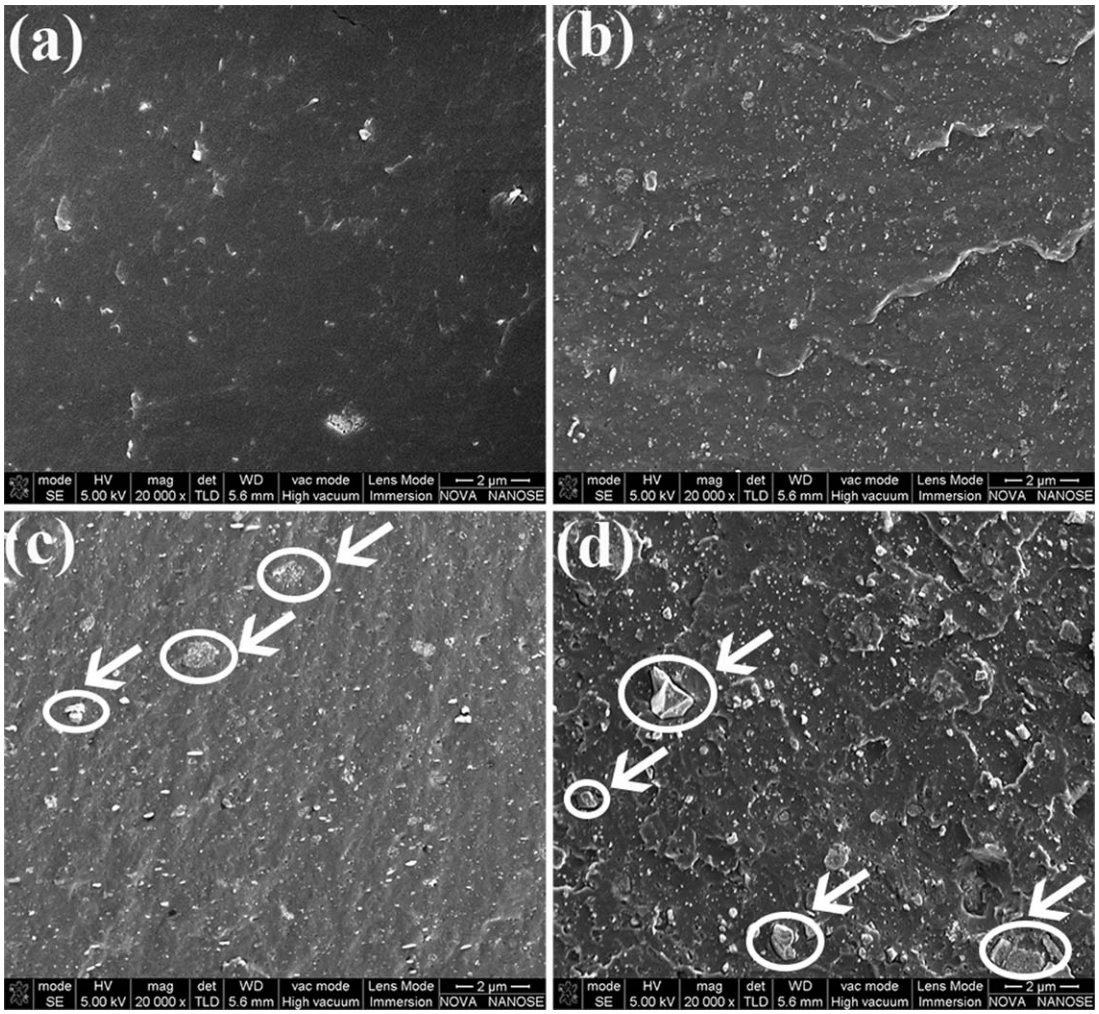

Figure 3. Dispersion of nano-$CaCO_3$ in the PPC matrix: (a) PPC-1, (b) PPC-3, (C) PPC-5, and (d) PPC-10. The arrows represent the aggregations of nano-$CaCO_3$.

and arrows. The SEM results reveal that the homogeneous dispersion of nano-$CaCO_3$ was achieved with 1 and 3 wt % PPC matrix.

Thermal Behavior of the PPC/Nano-$CaCO_3$ Composites

The thermal properties of the PPC and PPC/nano-$CaCO_3$ composites as measured by DSC are shown in Figure 4. The glass-transition temperature (T_g) data were taken as the end temperatures of the glass-transition region and are listed in Table I. The T_g of PPC-0 was about 26.7°C, whereas the T_g values of the PPC/nano-$CaCO_3$ composites were higher than that of the neat PPC. Moreover, the T_g values of the PPC/nano-$CaCO_3$ composites increased with increasing nano-$CaCO_3$ content. The T_g of the PPC/nano-$CaCO_3$ composite with 10 wt % $CaCO_3$ nanoparticles increased by 4.7°C compared with that of PPC-0. This was because the addition of nano-$CaCO_3$ reduced the mobility of the PPC chains.[30] However, we found that the improvement in T_g decreased when the nano-$CaCO_3$ content was higher than 3 wt %. This was because the aggregation of nano-$CaCO_3$ particles reduced the restriction to the chain mobility. Similar observations were reported elsewhere.[31]

TGA and differential thermogravimetry (DTG) curves of the PPC and PPC/nano-$CaCO_3$ composites are shown in Figure 5. The TGA and DTG analysis data are summarized in Table I. According to Figure 5(a), all of the samples exhibited one-step degradation behaviors, and the decomposition temperature (T_d) of PPC/nano-$CaCO_3$ composites shifted toward higher values. This revealed the PPC/nano-$CaCO_3$ composites achieved higher thermal stabilities than the neat PPC, and the thermal stability of the PPC/nano-$CaCO_3$ composites improved with increasing nano-$CaCO_3$ contents. It was reported that the nanoparticles, which uniformly dispersed in the polymer matrix, lead to a decrease in the heat conduction of the composites and acted as a mass-transport barrier to the volatile products that were generated during decomposition.[32–34] As a result, nano-$CaCO_3$ incorporated into the PPC matrix enhanced its thermal stability by acting as a superior thermal insulator; this is also known as the *shielding effect*.[35] However, the improvement in the percentage of T_d decreased as the nano-$CaCO_3$ content increased to 3 wt %, and T_d further decreased when the nano-$CaCO_3$ content exceeded 5 wt %. This was because the shielding effect became

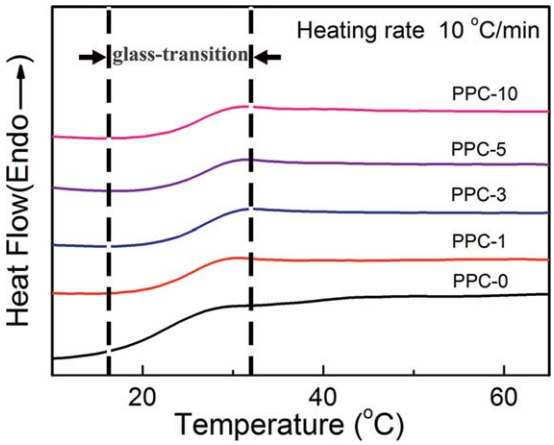

Figure 4. DSC curves of the neat PPC and PPC/nano-$CaCO_3$ composites with various nano-$CaCO_3$ contents. [Color figure can be viewed in the online issue, which is available at wileyonlinelibrary.com.]

weaker when the aggregation of nano-$CaCO_3$ occurred in the PPC matrix. Moreover, we noticed that the char residue of PPC-0 was 3.17 wt % because of the carbonization of the polymer under a nitrogen atmosphere. The char residue of the PPC nanocomposites tended to increase with increasing $CaCO_3$ content.

Rheological Behavior of the PPC/Nano-$CaCO_3$ Composites

The rheological behavior at low frequencies is very sensitive to the changing of the nanostructure/microstructure of filled polymer composites, so the formation of percolated filler networks and their associated pseudo-solid-like properties have often been studied in polymer/filler systems.[36–38] The percolated state of the nano-$CaCO_3$ could be detected by a sudden increase in G' as the behavior of the material becomes less dependent on the frequency as a function of the increased filler concentration. Figure 6(a–c) show the variations in η^*, dynamic G', and G'' with frequency as a function of ω. At low frequencies, G', G'' and η^* increased significantly with increasing nano-$CaCO_3$ content. It was interesting to note that the η^* of PPC-1 had a similar frequency dependency to that of PPC-0; this revealed a Newtonian plateau at low frequencies. However, the viscosity curves of PPC-3, PPC-5, and PPC-10 achieved a much steeper slope at low frequencies; this indicated that they exhibited a shear thinning effect during the entire frequency sweep. According to Figure 6(b), the low-frequency G' of the PPC nanocomposites also increased with the addition of nano-$CaCO_3$. When the nano-$CaCO_3$ contents increased up to 3 wt %, G' of these samples reached a plateau at low frequencies. The results indicate that the percolated nano-$CaCO_3$ may have formed a pseudo-solid-like network with strong interactions between the polymer and particles.[36] The onset of percolation could be more readily identified by the plotting of log G' versus log G'' [Figure 6(d)], which is known as a Han plot. The Han plot was used by Han and coworkers[39–41] to investigate temperature-induced changes in the microstructure of the homopolymers, block copolymers, and blends. In multiphase systems, the Han plot can be used in a similar way to indicate structural differences between the matrix and filled systems at a given temperature.[42,43] Any deviation from a linear relationship between G' and G'' is indicative of the formation of a percolated network. We clearly found that the curve for the PPC-3 composite deviated obviously from the linear relationship, and the deviation became more significant as the $CaCO_3$ content increased; this indicated the formation of nano-$CaCO_3$ filler networks with a PPC matrix. The filler networks within the polymer composites close to percolation threshold helped to achieve a uniform foam structure with a small cell diameter and high cell density.[44]

Effect of the Nano-$CaCO_3$ Content on the Foam Morphology

Figure 7 displays the SEM micrographs and cell diameter distribution of the PPC and PPC/nano-$CaCO_3$ composite foams. The foamed samples of neat PPC had separate, spherical, micrometer-sized cells with thick cell walls, and the cell diameter distribution obeyed a Gaussian distribution with a broad distribution width. When the addition of nano-$CaCO_3$ content was 3 wt %, the cell diameter decreased, and the cell density increased obviously. Meanwhile, the cell diameter distribution still obeyed a Gaussian distribution but with a narrower width. However, further increasing the nano-$CaCO_3$ content (5 and 10 wt %) led to a slight increase in the cell diameter and a decrease in the cell density, as shown in Figure 7(d,e).

The average cell diameters and cell densities calculated from the SEM micrographs are plotted in Figure 8. Compared with that of the PPC-0 foam, the cell diameters of PPC/nano-$CaCO_3$ composite foams decreased with increasing cell density. For instance, the average cell diameter decreased from 6.44 μm for the PPC-0 foam to 3.13 μm for the PPC-3 composite foam. At the same time, the cell density increased from 2.55×10^9 to 6.02×10^9 cells/cm^3. The reasons for these variations were attributed to the heterogeneous nucleation effects of nano-$CaCO_3$. During the foaming process, the nano-$CaCO_3$ served as

Table I. Thermal Properties of the Neat PPC and PPC/Nano-$CaCO_3$ Composites

Sample	T_g (°C)[a]	T_{onset} (°C)[b]	T_{max} (°C)[b]	Char residue at 600°C (wt %)
PPC-0	26.7 ± 0.2	231.5 ± 0.3	253.7 ± 0.2	3.17 ± 0.9
PPC-1	28.2 ± 0.3	232.7 ± 0.2	252.1 ± 0.5	5.25 ± 0.6
PPC-3	29.9 ± 0.1	245.9 ± 0.3	262.5 ± 0.2	6.08 ± 0.5
PPC-5	30.9 ± 0.3	245.1 ± 0.4	262.1 ± 0.3	8.80 ± 0.7
PPC-10	31.4 ± 0.2	246.3 ± 0.2	259.6 ± 0.4	12.39 ± 0.9

[a] T_g was recorded as the end temperature of the glass-transition region from the DSC curves.
[b] T_{onset}, initial decomposition temperature of thermal degradation; T_{max}, maximum weight loss temperature determined from DTG curves.

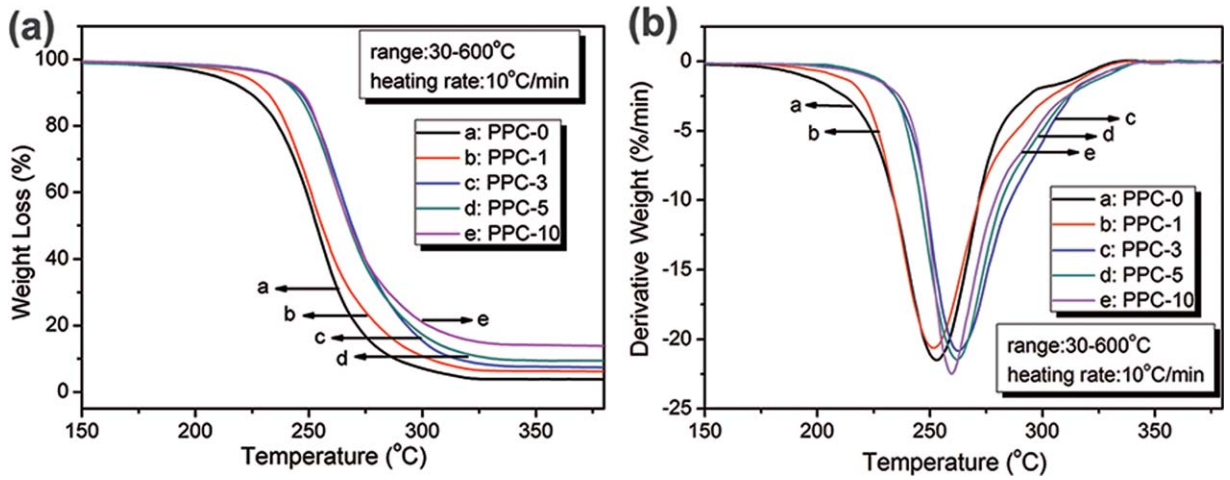

Figure 5. (a) TGA and (b) DTG curves of the neat PPC and PPC/nano-$CaCO_3$ composites. [Color figure can be viewed in the online issue, which is available at wileyonlinelibrary.com.]

heterogeneous nucleation sites where the cell nucleation took place at a low free energy. According to the heterogeneous nucleation theory, the added nano-$CaCO_3$ increased the number of nucleation sites and nucleation rate and decreased the cell diameter. Furthermore, the dispersion of nano-$CaCO_3$ in the matrix also significantly affected the cell diameter and structure. In general, a uniform dispersion of the nano-$CaCO_3$ particles may provide more nucleation sites to facilitate the cell nucleation and lead to a uniform cell structure.[45] According to Figure 3, when the nano-$CaCO_3$ content was 3 wt %, the nano-$CaCO_3$ was dispersed in the PPC matrix homogeneously; this indicated that 3 wt % nano-$CaCO_3$ provided more effective nucleation sites during foaming than other loading levels. As a result, the PPC-3 foam achieved a uniform microcellular structure with

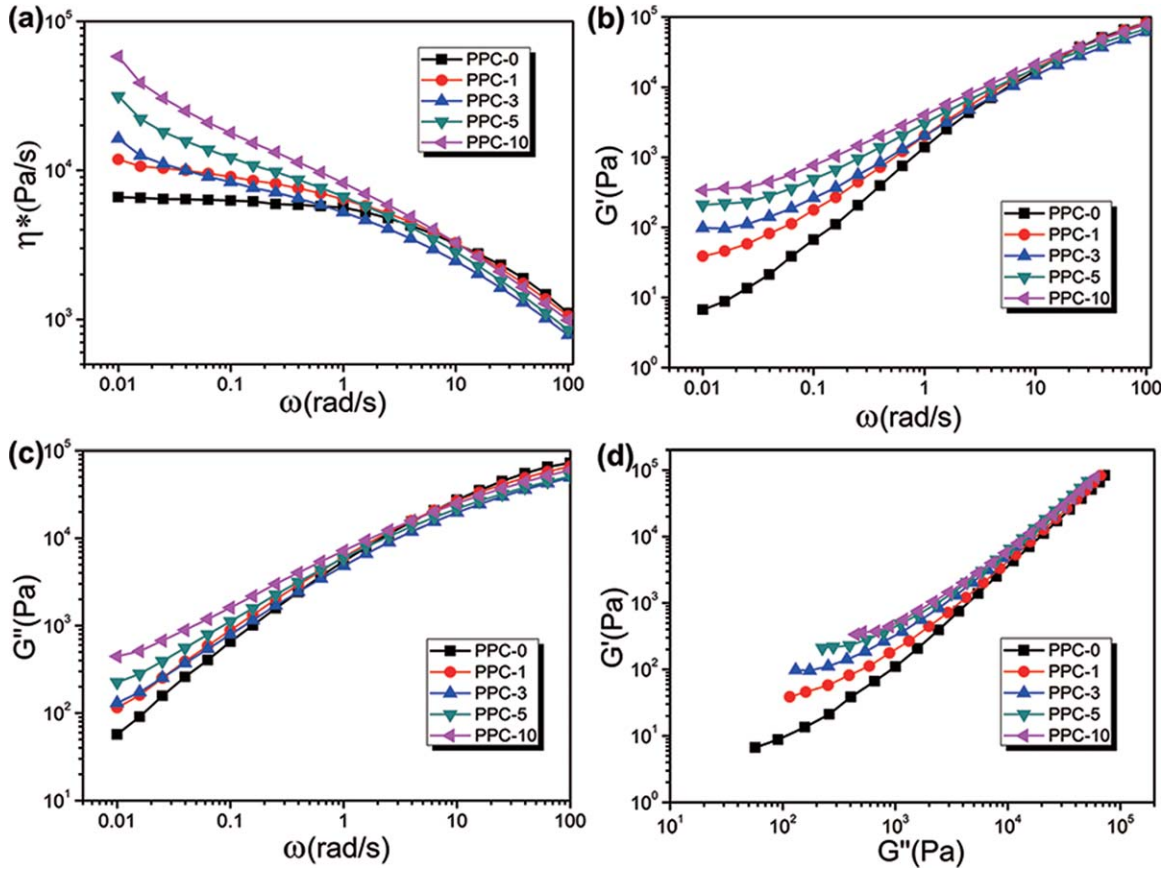

Figure 6. (a) η^*, (b) G', and (c) G'' of the neat PPC and PPC/nano-$CaCO_3$ composites as a function of ω at 150°C and (d) Han plots of G' versus G''. [Color figure can be viewed in the online issue, which is available at wileyonlinelibrary.com.]

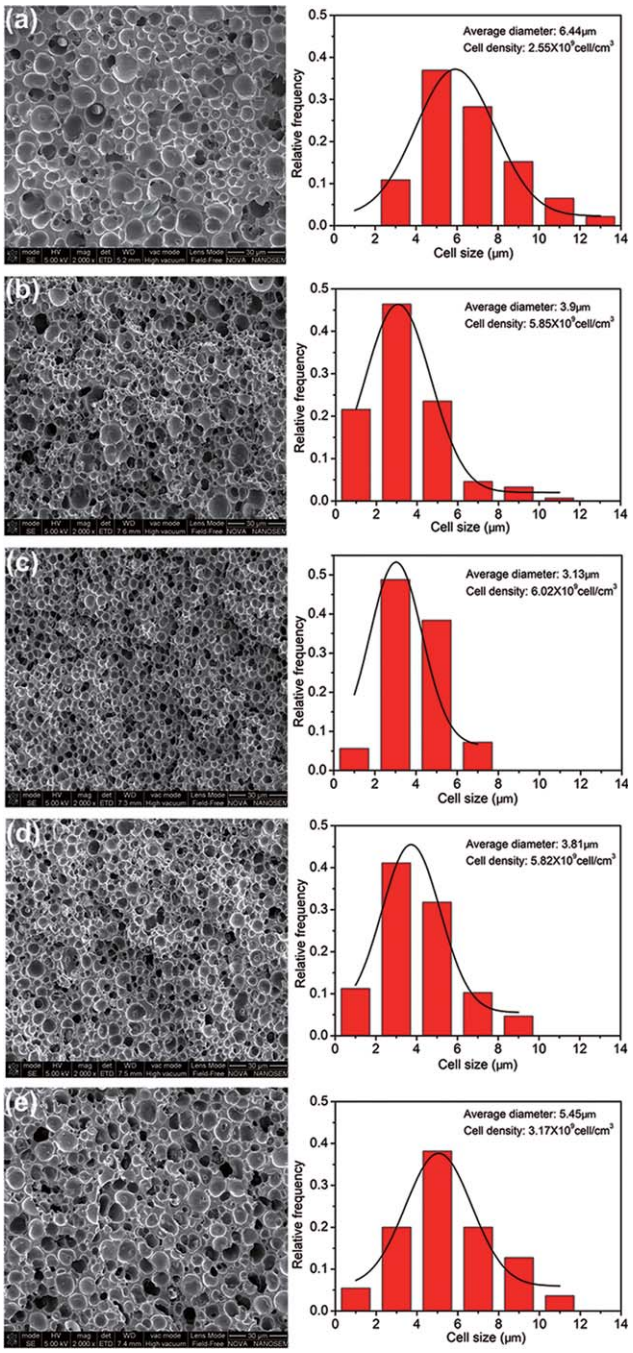

Figure 7. SEM images and cell diameter distribution of the neat PPC and PPC/nano-$CaCO_3$ composite foams: (a) PPC-0, (b) PPC-1, (c) PPC-3. (d) PPC-5, and (e) PPC-10. The P_s and foaming temperature were 10 MPa and 50°C, respectively. [Color figure can be viewed in the online issue, which is available at wileyonlinelibrary.com.]

narrow cell diameter distribution, small cell diameter, and large cell density. A further increase in the nano-$CaCO_3$ content up to 5 or 10 wt % led to a slight increase in the average cell diameter and a decrease in the cell density, especially for samples with 10 wt % nano-$CaCO_3$. The reason for this variation was that aggregated nano-$CaCO_3$ particles were like microparticles, which have a low surface-to-volume ratio, and the aggregates actually reduced the number of heterogeneous sites during foaming. This resulted in a low cell density. The observed result was consistent with the PP/nano-$CaCO_3$ composites, in which the aggregated nano-$CaCO_3$ caused larger cells and a lower cell density.[46]

Influence of the Pressure and Temperature on the Foam Morphology

The influence of the foaming conditions on the foam morphology of PPC-0 and PPC-3 were studied via a Taguchi test to investigate the effects of the foaming temperature and pressure on the cell structure because the dispersion of nano-$CaCO_3$ of PPC-3 was the best, and the filler content was close to the percolation threshold to form networks. Figure 9 shows the obtained morphologies and cell diameter distributions of the neat PPC at various foaming temperatures and pressures. The foams of all of the samples obtained a circular cell morphology, and their cell diameter distribution nearly obeyed a Gaussian distribution, except for the sample foamed at 10 MPa and 60°C. Noticeably, a uniform cell structure with the smallest average cell diameter (0.71 μm) and the largest cell density (2.09×10^{10} cells/cm^3) was achieved at foaming conditions of 20 MPa and 40°C. According to homogeneous nucleation theory,[47] as the magnitude of the pressure drop increased, the energy barrier to nucleation decreased. This led to more cells being nucleated. On the other hand, the viscosity of the PPC was higher at low temperatures, and this led to a retractive force sufficient to stop cell growth. In addition, the diffusivity of CO_2 within the PPC matrix was reduced at low temperature. These factors resulted in a homogeneous and small cell diameter. In contrast, the inhomogeneous and sparse cell structure was produced at foaming conditions of 10 MPa and 60°C. In general, the solubility of CO_2 in the polymer phase was decreased with increasing temperature or decreasing CO_2 pressure.[48] Therefore, the degree of supersaturation in the polymer phase was reduced, and this led to fewer nuclei been generated. Moreover, the higher the temperature was, the longer the time cells had to grow before vitrification. Therefore, larger cells could be formed at a low pressure and high temperature. The cell coalescence would be

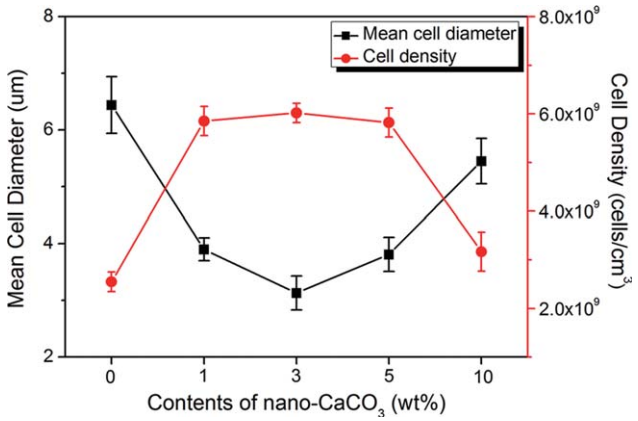

Figure 8. Cell diameter and cell density of the neat PPC and PPC/$CaCO_3$ composite foams with respect to the nano-$CaCO_3$ contents. [Color figure can be viewed in the online issue, which is available at wileyonlinelibrary.com.]

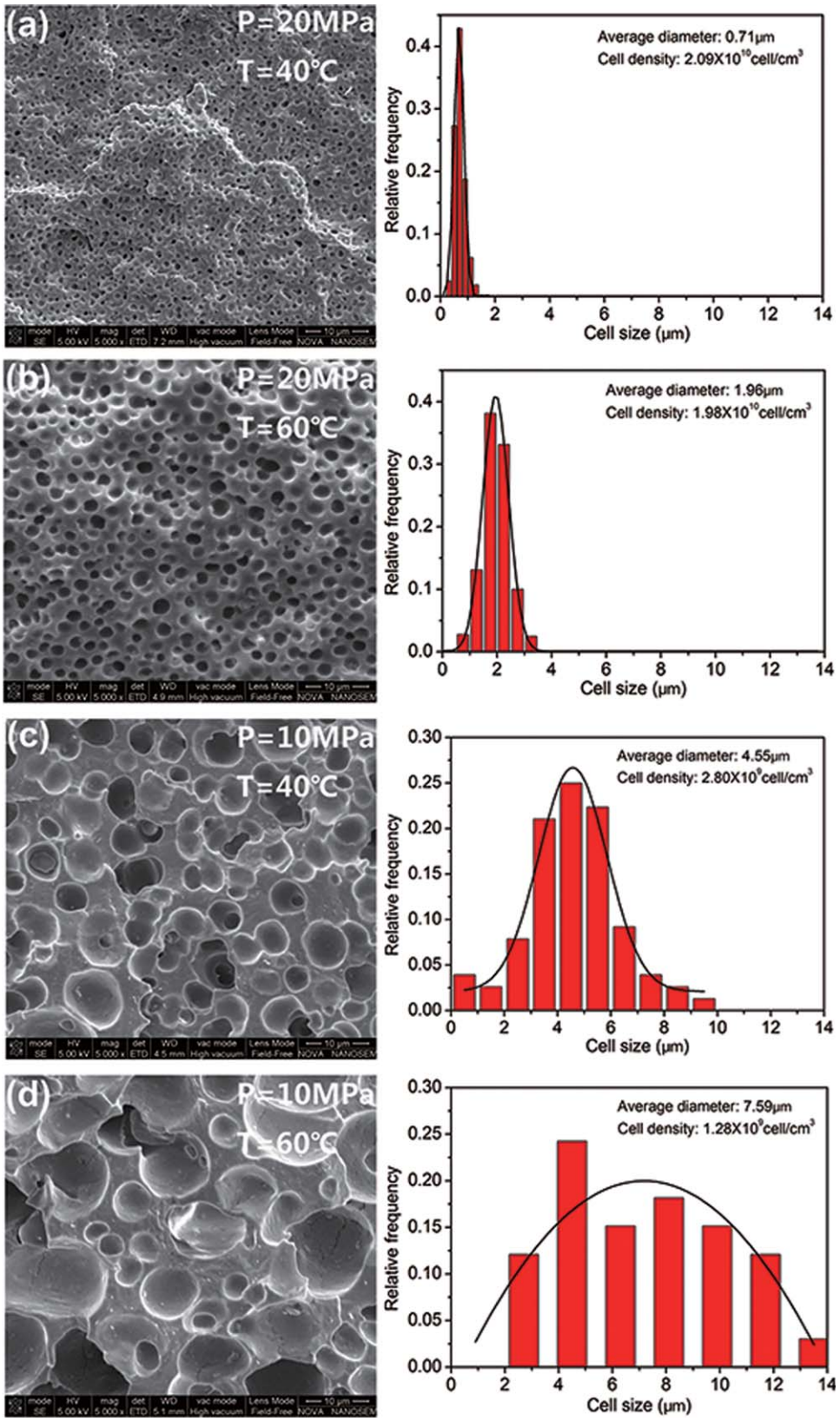

Figure 9. SEM images and cell diameter distribution of the PPC-0 foams under various foaming conditions of pressure (*P*) and temperature (*T*): (a) 20 MPa and 40°C, (b) 20 MPa and 60°C, (c) 10 MPa and 40°C, and (d) 10 MPa and 60°C. [Color figure can be viewed in the online issue, which is available at wileyonlinelibrary.com.]

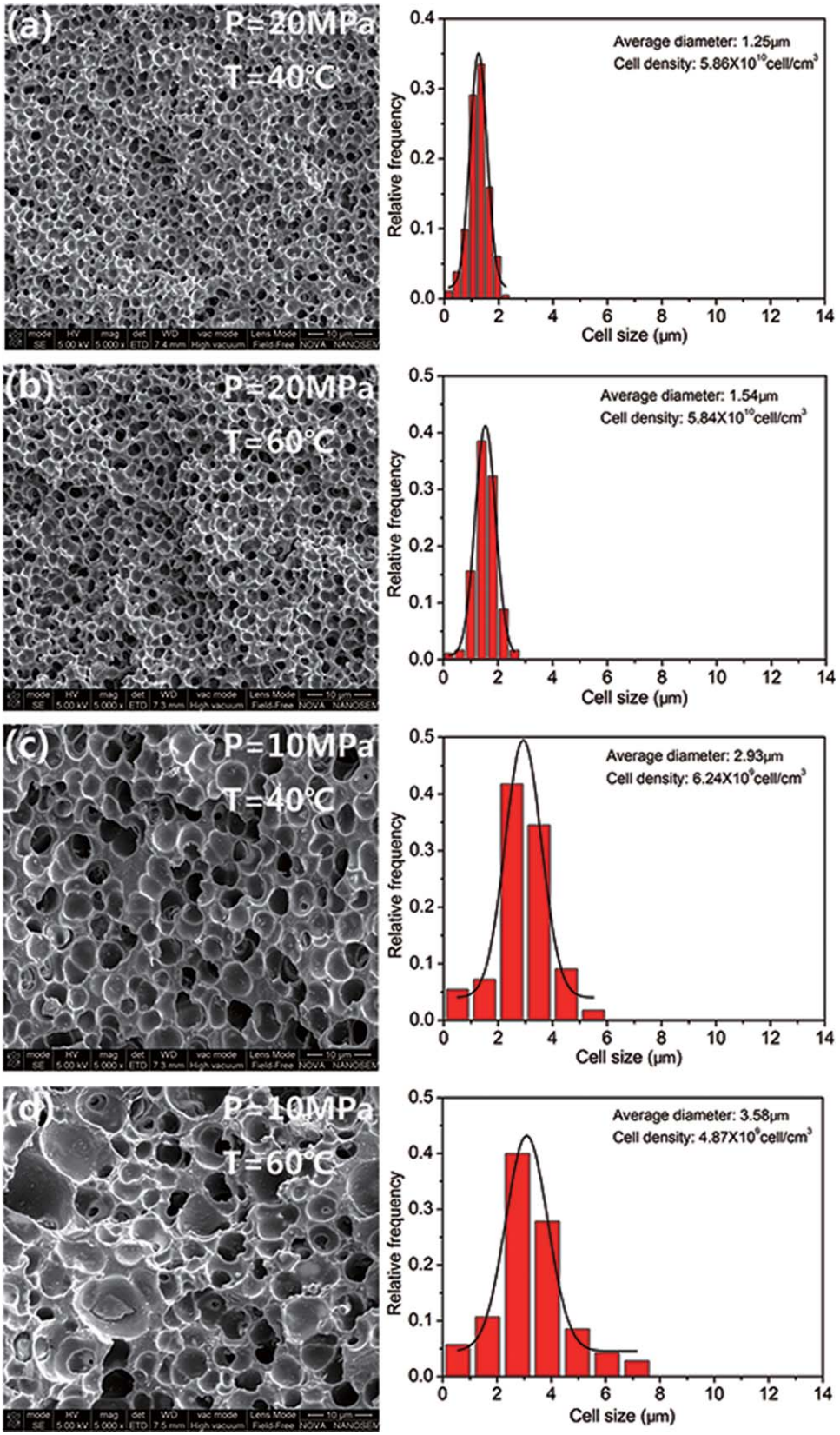

Figure 10. SEM images and cell diameter distribution of the PPC-3 foams under various foaming conditions of pressure (*P*) and temperature (*T*): (a) 20 MPa and 40°C, (b) 20 MPa and 60°C, (c) 10 MPa and 40°C, and (d) 10 MPa and 60°C. [Color figure can be viewed in the online issue, which is available at wileyonlinelibrary.com.]

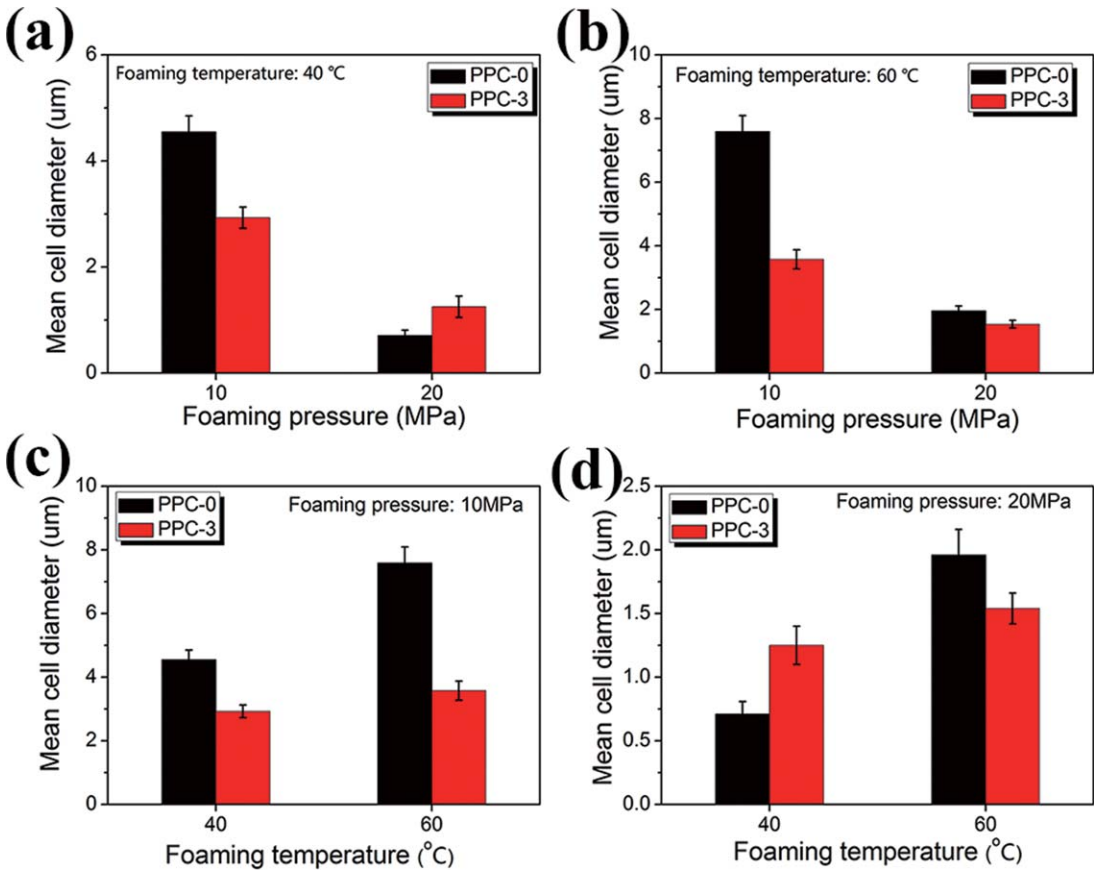

Figure 11. Effects of the foaming parameters (pressure and temperature) on the cell diameter of the PPC-0 foams and PPC-3 foams: (a) dependence on pressure at 40°C, (b) dependence on pressure at 60°C, (c) dependence on temperature at 10 MPa, and (d) dependence on temperature at 20 MPa. [Color figure can be viewed in the online issue, which is available at wileyonlinelibrary.com.]

another cause of the large cells because of the reduced PPC viscosity at high temperature.

Figure 10 shows the cell morphologies and cell diameter distributions of the PPC-3 foams at the same foaming conditions as PPC-0. We found from the results that the influences of the foaming conditions on the cell structure trends for PPC-3 were the same as PPC-0 for the same reasons demonstrated previously. However, in comparison with PPC-0, the foamability of the PPC-3 nanocomposite improved significantly. The PPC-3 foams showed more uniform structures under the corresponding foaming conditions, and the cell diameter distribution of all foamed samples obeyed a Gaussian distribution with a narrower width. As mentioned previously, the nano-$CaCO_3$ particles had large surface areas and could serve as heterogeneous nucleation sites; this resulted in the formation of cell embryos at a lower free energy during the foaming of the nanocomposites. As a result, an optimal cell structure with an average cell diameter of 1.25 μm and a cell density of 5.86×10^{10} cell/cm^3 for the PPC-3 foam was achieved at foaming conditions of 20 MPa and 40°C.

Figure 11 displays the relationship between the foaming parameters (pressure and temperature) and average cell diameter for the PPC-0 and PPC-3 foams. The average cell diameter as a function of the pressure is shown in Figure 11(a,b). We found that the cell diameter decreased as the pressure increased, and the cell diameter reduction of the PPC-0 foams was greater than that of the PPC-3 foams. For instance, the cell diameter of the PPC-0 foams decreased from 7.59 to 1.96 μm as the pressure increased from 10 to 20 MPa under 60°C, whereas the cell diameter of the PPC-3 foams decreased from merely 3.58 to 1.54 μm. This demonstrated that the PPC-0 foams were more sensitive to the pressure variations than the PPC-3 foams. The average cell diameter as a function of the temperature is shown in Figure 11(c,d). In the case of the temperature dependence of the cell diameter, the PPC-0 foams showed an apparent increase in the cell diameter with increasing temperature. However, the cell diameter of the PPC-3 foams increased scarcely from 1.25 to 1.54 μm with increasing temperature from 40 to 60°C at a P_s of 20 MPa. This suggests that at high P_s values, the processing temperature did not significantly affect the cell diameter of the PPC-3 foam. Even under low pressure (10 MPa), the average cell diameter of the PPC-3 foams increased only from 2.93 to 3.58 μm; these values corresponded to foaming temperatures of 40 and 60°C. The possible reason was that a rheological percolated filler network formed at 3 wt % nano-$CaCO_3$ content and was not destroyed under the foaming temperature range. The inversed conclusions were drawn from the cell density dependence on the foaming conditions for the PPC-0 foams, and the PPC-3 foams resulted because of the general concept that the larger the cell diameter was, the smaller the cell density was.

Therefore, the data are not shown. According to these results, we concluded that the cell structure dependence on the foaming pressure and temperature of the PPC-3 foams was weaker than those of the PPC-0 foams; this indicated that the PPC-3 foams had a higher structural stability. In addition, the change in the foaming pressure was more effective in altering the cell structure than the foaming temperature, and the dependence of the PPC-0 foams was stronger than that of PPC-3 foams.

CONCLUSIONS

In this study, the biodegradable foams were successfully prepared from the PPC/nano-$CaCO_3$ composites with sc-CO_2 as a physical blowing agent via batch foaming at various nano-$CaCO_3$ contents. The nano-$CaCO_3$ particles could achieve uniform dispersion at contents below 3 wt %. The addition of nano-$CaCO_3$ into the PPC matrix improved the thermal properties of PPC. Both the T_g and T_d values of the PPC/nano-$CaCO_3$ composites were found to be higher than those of neat PPC. Rheological tests revealed that the filler percolation threshold content to form networks within PPC matrix was 3 wt %. The foaming behavior studies of the composites indicated that the finest cell structure with a narrow cell diameter distribution was obtained at a 3 wt % nano-$CaCO_3$ content because of the homogeneous dispersion of nano-$CaCO_3$. As the nano-$CaCO_3$ content increased, the cell diameter increased as well because of the aggregation of the fillers. The cell structure dependence on the foaming conditions of the neat PPC and PPC/nano-$CaCO_3$ (3 wt %) composite was investigated. We found that the cell diameter reduction of the PPC-0 foams was greater than that of the PPC-3 foams when the pressure increased, and the PPC-0 foams showed a greater apparent increase in the cell diameter than the PPC-3 foams when the temperature increased. These results suggest that the PPC/nano-$CaCO_3$ composite had a higher structural stability at different conditions, and the influence of the foaming pressure on the cell structure was stronger than that of the foaming temperature.

ACKNOWLEDGMENTS

This work was supported by the National Science Foundation of China (contract grant numbers 51073061 and 21174044), the Guangdong Nature Science Foundation (contract grant number S2013020013855), and the National Basic Research Development Program 973 in China (contract grant number 2012CB025902).

REFERENCES

1. Corre, Y. M.; Maazouz, A.; Duchet, J.; Reignier, J. *J. Supercrit. Fluids* **2011**, *58*, 177.
2. Kuang, T. R.; Mi, H. Y.; Fu, D. J.; Jing, X.; Chen, B. Y.; Mou, W. J.; Peng, X. F. *Ind. Eng. Chem. Res.* **2015**, *54*, 758.
3. Xu, L. Q.; Huang, H. X. *Ind. Eng. Chem. Res.* **2014**, *53*, 2277.
4. Guan, L. T.; Xiao, M.; Meng, Y. Z.; Li, R. K. Y. *Polym. Eng. Sci.* **2006**, *46*, 153.
5. Guan, L. T.; Du, F. G.; Wang, G. Z.; Chen, Y. K.; Xiao, M.; Wang, S. J.; Meng, Y. Z. *J. Polym. Res.* **2007**, *14*, 245.
6. Zhong, X.; Dehghani, F. *Green Chem.* **2012**, *14*, 2523.
7. Reignier, J.; Gendron, R.; Champagne, M. F. *J. Cell. Plast.* **2007**, *43*, 459.
8. Peng, S. W.; An, Y. X.; Chen, C.; Fei, B.; Zhuang, Y. G.; Dong, L. S. *Polym. Degrad. Stab.* **2003**, *80*, 141.
9. Zhu, Q.; Meng, Y. Z.; Tjong, S. C.; Zhao, X. S.; Chen, Y. L. *Polym. Int.* **2002**, *51*, 1079.
10. Lai, M. F.; Li, J.; Liu, J. J. *J. Therm. Anal. Calorim.* **2005**, *82*, 293.
11. Gao, J.; Chen, F.; Wang, K.; Deng, H.; Zhang, Q.; Bai, H. W.; Fu, Q. *J. Mater. Chem.* **2011**, *21*, 17627.
12. Bian, J.; Wei, X. W.; Gong, S. J.; Zhang, H.; Guan, Z. P. *J. Appl. Polym. Sci.* **2012**, *123*, 2743.
13. Xu, J.; Li, R. K. Y.; Meng, Y. Z.; Mai, Y. W. *Mater. Res. Bull.* **2006**, *41*, 244.
14. Zhihao, Z.; Joong-Hee, L.; Seok-Bong, H.; Pittman, C. U. *Jr. Polymer* **2008**, *49*, 2947.
15. Li, X. H.; Meng, Y. Z.; Wang, S. J.; Rajulu, A. V.; Tjong, S. C. *J. Polym. Sci. Part B: Polym. Phys.* **2004**, *42*, 666.
16. Chen, W. F.; Pang, M. Z.; Xiao, M.; Wang, S. J.; Wen, L. S.; Meng, Y. Z. *J. Reinforced Plast. Compos.* **2010**, *29*, 1545.
17. Li, X. H.; Tjong, S. C.; Meng, Y. Z.; Zhu, Q. *J. Polym. Sci. Part B: Polym. Phys.* **2003**, *41*, 1806.
18. Tang, C. Y.; Chan, L. C.; Liang, J. Z.; Cheng, K. W. E.; Wong, T. L. *J. Reinforced Plast. Compos.* **2002**, *21*, 1337.
19. Baskaran, R.; Sarojadevi, M.; Vijayakumar, C. T. *J. Reinforced Plast. Compos.* **2011**, *30*, 1549.
20. Huang, H. X.; Wang, J. K. *J. Appl. Polym. Sci.* **2007**, *106*, 505.
21. Liu, H.; Han, C.; Dong, L. *Polym. Compos.* **2010**, *31*, 1653.
22. Ding, J.; Shangguan, J.; Ma, W.; Zhong, Q. *J. Appl. Polym. Sci.* **2013**, *128*, 3639.
23. Jiao, J.; Xiao, M.; Shu, D.; Li, L.; Meng, Y. Z. *J. Appl. Polym. Sci.* **2006**, *102*, 5240.
24. Arora, K. A.; Lesser, A. J.; McCarthy, T. *J. Macromolecules* **1998**, *31*, 4614.
25. Miller, D.; Chatchaisucha, P.; Kumar, V. *Polymer* **2009**, *50*, 5576.
26. Corre, Y. M.; Maazouz, A.; Duchet, J.; Reignier, J. *J. Supercrit. Fluids* **2011**, *58*, 177.
27. Wang, W. Y.; Zeng, X. F.; Wang, G. Q.; Chen, J. F. *J. Appl. Polym. Sci.* **2007**, *106*, 1932.
28. Bellayer, S.; Tavard, E.; Duquesne, S.; Piechaczyk, A.; Bourbigot, S. *Polym. Degrad. Stab.* **2009**, *94*, 797.
29. Wan, W.; Yu, D.; Xie, Y.; Guo, X.; Zhou, W.; Cao, J. *J. Appl. Polym. Sci.* **2006**, *102*, 3480.
30. Di Lorenzo, M. L.; Errico, M. E.; Avella, M. *J. Mater. Sci.* **2002**, *37*, 2351.
31. Pal, M.; Singh, B.; Gautam, J. *J. Therm. Anal. Calorim.* **2012**, *107*, 85.
32. Bian, J.; Wei, X. W.; Gong, S. J.; Zhang, H.; Guan, Z. P. *J. Appl. Polym. Sci.* **2012**, *123*, 2743.

33. Xu, J.; Li, R. K. Y.; Meng, Y. Z.; Mai, Y. W. *Mater. Res. Bull.* **2006**, *41*, 244.
34. Zhihao, Z.; Joong-Hee, L.; Seok-Bong, H.; Pittman, C. U. *Jr. Polymer* **2008**, *49*, 2947.
35. Pal, M.; Gautam, J. *J. Therm. Anal. Calorim.* **2013**, *111*, 689.
36. Li, Y.; Han, C.; Bian, J.; Han, L.; Dong, L.; Gao, G. *Polym. Compos.* **2012**, *33*, 1719.
37. Pötschke, P.; Fornes, T. D.; Paul, D. R. *Polymer* **2002**, *43*, 3247.
38. Kota, A. K.; Cipriano, B. H.; Duesterberg, M. K.; Gershon, A. L.; Powell, D.; Raghavan, S. R.; Bruck, H. A. *Macromolecules* **2007**, *40*, 7400.
39. Han, C. D.; Lem, K. W. *Polym. Eng. Rev.* **1983**, *2*, 135.
40. Chuang, H. K.; Han, C. D. *J. Appl. Polym. Sci.* **1984**, *29*, 2205.
41. Han, C. D.; Kim, J.; Kim, J. K. *Macromolecules* **1989**, *22*, 383.
42. Han, C. D.; Kim, J. *J. Polym. Sci. Part B: Polym. Phys.* **1987**, *25*, 1741.
43. McClory, C.; McNally, T.; Baxendale, M.; Potschke, P.; Blau, W.; Ruether, M. *Eur. Polym. J.* **2010**, *46*, 854.
44. Di, Y.; Iannace, S.; Maio, E. D.; Nicolais, L. *J. Polym. Sci. Part B: Polym. Phys.* **2005**, *43*, 689.
45. Ding, J.; Ma, W.; Song, F.; Zhong, Q. *J. Mater. Sci.* **2013**, *48*, 2504.
46. Ding, J.; Ma, W.; Song, F.; Zhong, Q. *J. Mater. Sci.* **2013**, *48*, 2504.
47. Goel, S. K.; Beckman, E. *J. Polym. Eng. Sci.* **1994**, *34*, 1137.
48. Han, X.; Koelling, K. W.; Tomasko, D. L.; Lee, L. *J. Polym. Eng. Sci.* **2003**, *43*, 1206.